J. Phys.: Condens. Matter **25** (2013) 445801 (8pp) doi:10.1088/0953-8984/25/44/445801

Thermal transport across metal–insulator interface via electron–phonon interaction

Lifa Zhang[1], Jing-Tao Lü[2], Jian-Sheng Wang[1] and Baowen Li[1,3,4]

[1] Department of Physics and Centre for Computational Science and Engineering, National University of Singapore, Singapore 117542, Republic of Singapore
[2] School of Physics, Huazhong University of Science and Technology, Wuhan, 430074, People's Republic of China
[3] NUS Graduate School for Integrative Sciences and Engineering, Singapore 117456, Republic of Singapore
[4] Center for Phononics and Thermal Energy Science, School of Physics Science and Engineering, Tongji University, Shanghai 200092, People's Republic of China

E-mail: phylibw@nus.edu.sg (Baowen Li)

Received 14 August 2013, in final form 9 September 2013
Published 16 October 2013
Online at stacks.iop.org/JPhysCM/25/445801

Abstract
The thermal transport across a metal–insulator interface can be characterized by electron–phonon interaction through which an electron lead is coupled to a phonon lead if phonon–phonon coupling at the interface is very weak. We investigate the thermal conductance and rectification between the electron part and the phonon part using the nonequilibrium Green's function method. It is found that the thermal conductance has a nonmonotonic behavior as a function of average temperature or the coupling strength between the phonon leads in the metal part and the insulator part. The metal–insulator interface shows a clear thermal rectification effect, which can be reversed by a change in average temperature or the electron–phonon coupling.

(Some figures may appear in colour only in the online journal)

1. Introduction

With the increase of integration density, accumulation of heat becomes a bottleneck for the further development of microelectronic devices. Moreover, as most electronic devices consist of metal and insulator/semiconductor interfaces, an understanding of the thermal transport through the metal–insulator/semiconductor interface is indispensable for work on heat dissipation [1–3].

Electrons dominate thermal transport in metals while phonons dominate in semiconductors and insulators; thus for thermal transport across metal–nonmetal interfaces, energy must transfer between electrons and phonons [4]. Thanks to its many remarkable physical properties and potential for large-area epitaxial growth, graphene is a promising material for future electronics [5]. Biased graphene on a dielectric insulator often appears in electronic devices especially in transistors. Due to the bias the electrons in the metallic part have a higher effective temperature than the phonons in the insulating substrate, and the thermal transport from the electrons in metal to the phonons in insulator is an important channel of energy transfer [7, 8]. It was found in a very recent experiment on a carbon nanotube that more that 80% of the electrical power supplied to the nanotube is transferred directly into the substrate by the electron–phonon interaction (EPI) [9]. Therefore to understand the thermal transport across the interface through the EPI is highly desirable for progress on heat dissipation in electronic devices.

To study the thermal transport across the interface, the acoustic mismatch model [6] and the diffuse mismatch model [10, 4] are widely applied; however, both models offer limited accuracy in nanoscale interfacial resistance predictions [11] because they neglect the atomic details of actual interfaces. A scattering boundary method within the lattice dynamic approach [12–14] fully considers the atomic structures in the interface; but it can only be applied to ballistic thermal transport. Classical molecular dynamics is another widely used method in phonon transport [15–17], which is not accurate below the Debye temperature, and ignores the quantum effect. Only recently has the nonequilibrium

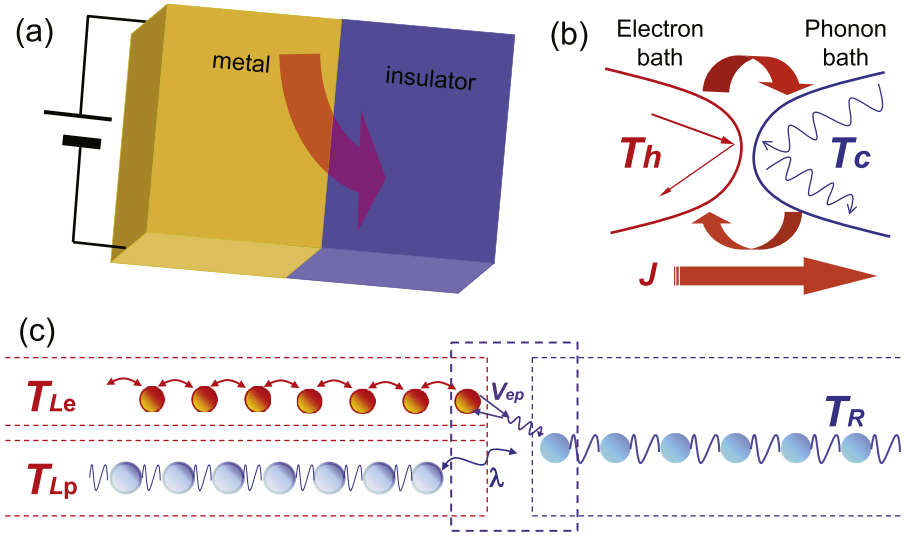

Figure 1. (a) Heat generation in a metal with an applied bias. The arrow shows the heat transport from the metal to the insulating substrate. (b) An electron bath and a phonon bath at two different temperatures connected by EPI. Energy exchanges between the two baths and there is a net thermal current J from the hot bath to the cold one. (c) The lattice model of the metal–insulator interface. The one-dimensional electron lead (the left upper semi-infinite chain where the dots represent electron states) connects to the one-dimensional atomic chain (the right semi-infinite chain) via electron–phonon interaction V_{ep}. The phonon part in the metal (the left lower semi-infinite atomic chain) can also be considered to contribute to the thermal transport, which connects to the right atomic chain by a relative coupling λ.

Green's function method, which originates from the study of electronic transport [18], been applied to study the quantum phonon transport [19–22]. To date, the study of the coupled electronic and phonon transport [23–25] is rare, especially in the metal–nonmetal interface [4, 26, 27].

In this paper, using the nonequilibrium Green's function method, we study the thermal transport across the metal–insulator interface via the EPI. Our model can also be applied to the metal–semiconductor interface. We study energy flow between an electron bath and a phonon bath which are connected by electron–phonon coupling, as shown in figure 1(b). The electron bath, described by a semi-infinite electronic chain under tight-binding approximation, connects with a phonon lead illustrated as a semi-infinite harmonic atomic chain by a weak EPI, as shown in figure 1(c), where the phonon degrees of freedom in metal can also be considered in the thermal transport.

2. Model and method

We study the interfacial thermal transport at the metal–insulator interface as shown in figure 1(a). To manifest the effect of the interface we exclude the nonlinear electron or phonon transport in the two materials themselves, thus the only thermal resistance comes from the interface. Such model really uncovers the thermal transport properties of the interface itself. To study the longitudinal thermal transport, that is, the cross-plane interfacial transport, we can simplify the problem further to thermal transport between an electron bath and a phonon bath which are connected by an electron–phonon coupling, as shown in figure 1(b), and which can be represented by a one-dimensional lattice model as shown in figure 1(c), where a semi-infinite electronic chain (at temperature T_{Le}) is connected to a semi-infinite atomic chain (at temperature T_R) by an EPI V_{ep}. The phonon part in the metal can also be considered as another semi-infinite atomic chain which connects to the right atomic chain by a relative coupling λ. In our model, the scattering for both electrons and phonons only comes from the interface, and the electron and phonon transport in the corresponding semi-infinite periodic leads is ballistic. Therefore we can partition the system into three parts (L, C, R), the atoms at the interface are regarded as at the center, illustrated as the dashed-line rectangle in figure 1(c), and the remaining parts are leads. For simplicity, we only consider the one-dimensional case, ignoring electron spin. Thus the Hamiltonian of the whole system in figure 1(c) is written as

$$H = H_{\mathrm{e}}^{\mathrm{L}} + H^{\mathrm{C}} + H_{\mathrm{e}}^{\mathrm{LC}} + \sum_{\alpha=\mathrm{L,R}} (H_{\mathrm{p}}^{\alpha} + H_{\mathrm{p}}^{\alpha\mathrm{C}}), \qquad (1)$$

where $H_{\mathrm{e}}^{\mathrm{L}} = \sum_i \varepsilon_0 c_i^{\dagger} c_i - \sum_{|i-j|=1} t c_i^{\dagger} c_j$ is the Hamiltonian of the electron lead in the left part. The electron coupling between the left lead (site 1) and the center is $H_{\mathrm{e}}^{\mathrm{LC}} = -t c_1^{\dagger} c - t c^{\dagger} c_1$. We set atomic mass to $m = 1$, and the Hamiltonian of the center is

$$H^{\mathrm{C}} = \tfrac{1}{2}\dot{u}^2 + \tfrac{1}{2}(\lambda k^{\mathrm{L}} + k^{\mathrm{R}})u^2 + \varepsilon_0 c^{\dagger} c + V_{\mathrm{ep}} c^{\dagger} c u, \qquad (2)$$

where k^{L} and k^{R} are the spring constants of the left and right atomic chains, respectively. u is the atom displacement. λk^{L} denotes the coupling between the two atomic chains; λ can be chosen from 0 to 1. V_{ep} is the electron–phonon coupling. The phonon Hamiltonian of the two leads and its coupling to the center are $H_{\mathrm{p}}^{\alpha} = \frac{1}{2}\sum_i \dot{u}_i^{\alpha}\dot{u}_i^{\alpha} + \frac{1}{2}\sum_{|i-j|=0,1} u_i^{\alpha} K_{ij}^{\alpha} u_j^{\alpha}$ and $H_{\mathrm{p}}^{\alpha\mathrm{C}} = u_1^{\alpha} K^{\alpha\mathrm{C}} u$ [20, 23].

Applying the standard procedure of the nonequilibrium Green's function method [20], without the EPI, we obtain the electron retarded Green's function $G_0^{\mathrm{r}}(\varepsilon) = \left[\varepsilon - \varepsilon_0 - \Sigma_{\mathrm{L}}^{\mathrm{r}}(\varepsilon)\right]^{-1}$, where $\Sigma_{\mathrm{L}}^{\mathrm{r}} = g_{\mathrm{L}}^{\mathrm{r}} t^2$ is the retarded

self-energy with a surface Green's function $g^{\rm r}_{\rm L}$, where $g^{\rm r} = \left[(\varepsilon + {\rm i}\eta)I - H^{\rm L}_{\rm e}\right]^{-1}$. The lesser Green's function can also be easily obtained. The phonon retarded Green's functions is $D^{\rm r}_0(\omega) = D^{a\dagger}_0(\omega) = \left[\omega^2 - (\lambda k^{\rm L} + k^{\rm R}) - \Pi^{\rm r}_{\rm L}(\omega) - \Pi^{\rm r}_{\rm R}(\omega)\right]^{-1}$, where $\Pi^{\rm r}_{\rm L}(\omega) = (\lambda k^{\rm L})^2 d^{\rm r}_{\rm L}(\omega)$ and $\Pi^{\rm r}_{\rm R}(\omega) = (k^{\rm R})^2 d^{\rm r}_{\rm R}(\omega)$ are the retarded self-energies of left and right leads with surface Green's function $d^{\rm r}_{\rm L}$ and $d^{\rm r}_{\rm R}$, where $d^{\rm r}_{\rm L,R} = \left[(\omega + {\rm i}\eta)^2 I - K^{\rm L,R}\right]^{-1}$. The EPI is included as perturbation. The full Green's functions are obtained from the Dyson equation, that is, $G^{{\rm r},a} = [(G^{{\rm r},a}_0)^{-1} - \Sigma^{{\rm r},a}_{\rm ep}]^{-1}$, and $G^{<,>} = G^{\rm r}(\Sigma^{<,>}_{\rm ep} + \Sigma^{<,>}_{L})G^a$, where $\Sigma^{{\rm r},a,<,>}_{\rm ep}$ is the self-energy from the EPI. For phonons, we have $D^{{\rm r},a} = [(D^{{\rm r},a}_0)^{-1} - \Pi^{{\rm r},a}_{\rm ep}]^{-1}$, and $D^{<,>} = D^{\rm r}(\Pi^{<,>}_{\rm ep} + \Pi^{<,>}_{L} + \Pi^{<,>}_{R})D^a$, where the nonlinear self-energy $\Pi^{{\rm r},a,<,>}_{\rm ep}$ comes from the electron–phonon coupling. Keeping the lowest nonzero order (second order) of the self-energies, we obtain the nonlinear self-energies $\Sigma^{{\rm r},a,<,>}_{\rm ep}$ and $\Pi^{{\rm r},a,<,>}_{\rm ep}$ up the second order, which are general for any dimensional systems. For our one-dimensional simple model as shown in equation (2), the self-energies can be written as

$$\Sigma^{>,<}_{\rm ep}(\varepsilon) = {\rm i}V^2_{\rm ep}\int G^{>,<}_0(\varepsilon - \omega)D^{>,<}_0(\omega)\frac{{\rm d}\omega}{2\pi}, \tag{3}$$

and

$$\begin{aligned}\Sigma^{\rm r}_{\rm ep}(\varepsilon) = {\rm i}V^2_{\rm ep}\Bigg\{&-D^{\rm r}_0(\omega' = 0)\int G^{<}_0(\varepsilon')\frac{{\rm d}\varepsilon'}{2\pi}\\ &+ \int\frac{{\rm d}\omega}{2\pi}\big[G^{\rm r}_0(\varepsilon - \omega)D^{<}_0(\omega) + G^{<}_0(\varepsilon - \omega)\\ &\times D^{\rm r}_0(\omega) + G^{\rm r}_0(\varepsilon - \omega)D^{\rm r}_0(\omega)\big]\Bigg\}.\end{aligned} \tag{4}$$

The nonlinear self-energies for the phonons are

$$\Pi^{>,<}_{\rm ep}(\omega) = -{\rm i}V^2_{\rm ep}\int\frac{{\rm d}\varepsilon}{2\pi}G^{>,<}_0(\varepsilon)G^{<,>}_0(\varepsilon - \omega), \tag{5}$$

and

$$\begin{aligned}\Pi^{\rm r}_{\rm ep}(\omega) = -{\rm i}V^2_{\rm ep}\int\frac{{\rm d}\varepsilon}{2\pi}\big[&G^{\rm r}_0(\varepsilon)G^{<}_0(\varepsilon - \omega)\\ &+ G^{<}_0(\varepsilon)G^{a}_0(\varepsilon - \omega)\big].\end{aligned} \tag{6}$$

Equations (3)–(6) are the so-called Born approximation (BA). By replacing the bare Green's functions G_0 and D_0 with the full Green's functions G and D, we perform iteration under the self-consistent Born approximation (SCBA). While the BA fails to satisfy the energy current conservation, the SCBA fulfils it [23].

Therefore, we obtain the heat current from the electron part as [18, 28, 29]

$$J^{\rm e} = \int\frac{{\rm d}\varepsilon}{2\pi\hbar}\,\varepsilon\,{\rm Tr}\{G^{>}(\varepsilon)\Sigma^{<}_{\rm L}(\varepsilon) - G^{<}(\varepsilon)\Sigma^{>}_{\rm L}(\varepsilon)\}. \tag{7}$$

The heat current from the phonon lead is [20, 23, 30]

$$J^{\rm p}_{\alpha} = -\int\frac{{\rm d}\omega}{4\pi}\,\hbar\omega\,{\rm Tr}\{D^{>}(\omega)\Pi^{<}_{\alpha}(\omega) - D^{<}(\omega)\Pi^{>}_{\alpha}(\omega)\}. \tag{8}$$

Due to energy conservation, $J^{\rm e} + J^{\rm p}_{\rm L} + J^{\rm p}_{\rm R} = 0$. If the coupling $\lambda = 0$, we obtain $J^{\rm e} = -J^{\rm p}_{\rm R}$ when the energy flows across the interface only through EPI, that is, the heat generation of the metal part transfers directly to the insulator part. We set the Planck constant $\hbar = 1$ and the Boltzmann constant $k_{\rm B} = 1$ in the following numerical calculation; and $\varepsilon_0 = 0$, $k^{\rm L} = k^{\rm R} = 1$, $t = 1$. We define the conductance $\sigma = |J^{\rm e}|/\Delta T$ to illustrate the thermal transport between the electron part and the phonon part.

3. Thermal conductance across the interface

As shown in figure 1(a), if the metal part has a voltage applied, the average energy of electrons increases, which means that the electrons have a higher effective temperature than the phonons. Thus we set the left and right phonon leads to a lower temperature $T_{L{\rm p}} = T_R = T_0 - \Delta T$, while the electron lead has a higher temperature $T_{L{\rm e}} = T_0 + \Delta T$. If we do not consider the phonon contribution in the metal part, the thermal conductance from the electron lead to the phonon lead has a nonmonotonic behavior with increasing of average temperature T_0, as shown in figure 2(a). In the low-temperature region, as temperature increases, the thermal conductance increases due to a greater contribution from electrons with energy far from the Fermi surface ($\varepsilon = 0$) although there is a certain decrease in the contribution from near the Fermi surface, which can be seen from the solid line ($T_0 = 0.2$) and dashed line ($T = 0.6$) in figure 2(b). With the temperature further increasing, the dominating effect comes from the decrease of the contribution near the Fermi level, as shown by the dashed line and dotted line of figure 2(b). This causes the thermal conductance to decrease after a certain temperature. Such dependence of thermal conductance on temperature is consistent with the experimental observation of thermal contact conductance between graphene and silicon dioxide [31]. While the conductance has a nonmonotonic dependence on T_0, the heat current and conductance shows a monotonic behavior with temperature difference ΔT increasing, as shown in the inset of figure 2(c). If we include the phonon contribution in the metal part, the thermal conductance has a similar temperature dependence, but with a smaller magnitude. This means that the heat generation from the electron part is affected by the coupling strength between the two phonon parts in the metal–insulator interface.

In order to investigate the effect of phonon–phonon channel λ on the thermal transport through the electron–phonon channel $V_{\rm ep}$, in figure 3(a) we plot the heat current from the electrons to the phonons when we increase the coupling strength λ between the two phonon parts. We find that in the small λ region, with λ increasing the heat current flowing into the right phonon lead will increase due to the smaller difference between the atom ($K^{\rm C} = (\lambda k^{\rm L} + k^{\rm R})$) in interface and the atoms ($K^{\rm R}_{ii} = 2k^{\rm R}$) in the right lead, and thus the scattering for phonons at the interface decreases. The heat transports more easily to the right lead; $J^{\rm e}$ increases. At the same time, heat can flow from the electrons to the left phonon lead; $-J^{\rm p}_{\rm L}$ increases with λ. When λ increases

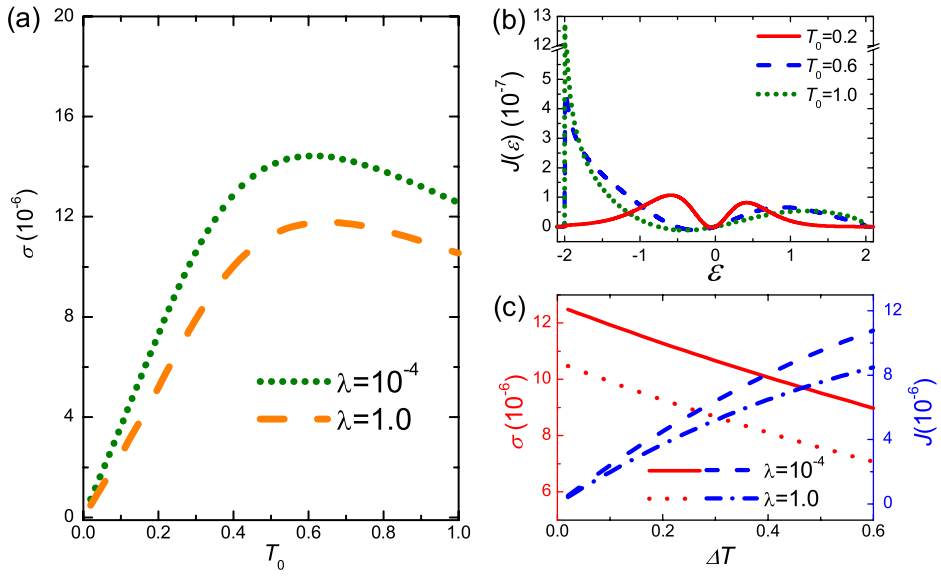

Figure 2. (a) Thermal conductance across the metal–insulator interface versus the average temperature of the baths. $T_{Le} = T_0 + \Delta T$, $T_{Lp} = T_R = T_0 - \Delta T$, $\Delta T = 0.01$, and $V_{ep} = 0.01$. (b) The thermal current density $J(\varepsilon)$ ($J^e = \int d\varepsilon\, J(\varepsilon)$) for electrons with energy ε at $\lambda = 0^+ = 10^{-4}$. (c) The thermal conductance (left scale) and current (right scale) from the electron bath versus the temperature difference ΔT at $T_0 = 1.0$.

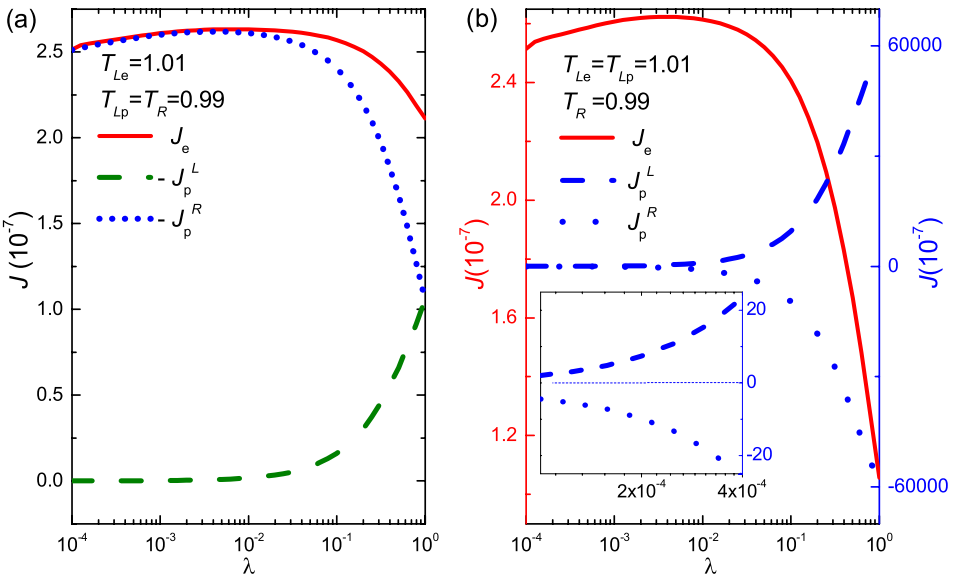

Figure 3. (a) Thermal current versus the coupling λ. The solid line corresponds to the thermal current J^e flowing from the electron bath. The dashed and dotted lines correspond to the thermal current ($-J_L^p$ and $-J_R^p$) flowing into the left and right phonon baths, respectively. (b) Thermal current versus the coupling λ at $T_{Le} = T_{Lp} = 1.01$, $T_R = 0.99$. The solid, dashed and dotted lines correspond to the thermal current flowing from the electron bath (left scale), the left and the right phonon baths (right scale), respectively. The inset shows a close-up of (b) for small λ. For (a) and (b), $V_{ep} = 0.01$.

further, the phonon scattering between the left chain and the center atom decreases, and thermal energy transfers from the electron more easily into the left lead. Such fast increase of $-J_L^p$ causes a decreasing of the heat flow into the right lead $-J_R^p$. With increasing λ, the phonon scattering at the interface between the left and right atomic chains decreases, more phonons can transport coherently in the two atomic leads, and couple less efficiently to electrons; thus the heat flowing from the electron lead begins to decrease. Due to the continuous increase of the heat flowing into the left phonon lead $-J_L^p$, and $J^e + J_L^p + J_R^p = 0$, thus the decrease of heat from electrons J^e lags behind the decrease of the heat flow into the right lead $-J_R^p$. If $\lambda = 1$, the heat flow into the two phonon leads has the same value due to the symmetry. As shown in figure 3(b), if the non-biased metal part is at a higher temperature while the insulator is at a lower one, the heat flow from the electron part has a similar dependence on λ; but the heat flowing from the left phonon lead and the one into the right phonon lead monotonically increase with λ since phonon transport dominates heat flow in such a case and the phonon scattering decreases. We also find that in this case the thermal transport through the phonon–phonon channel λ

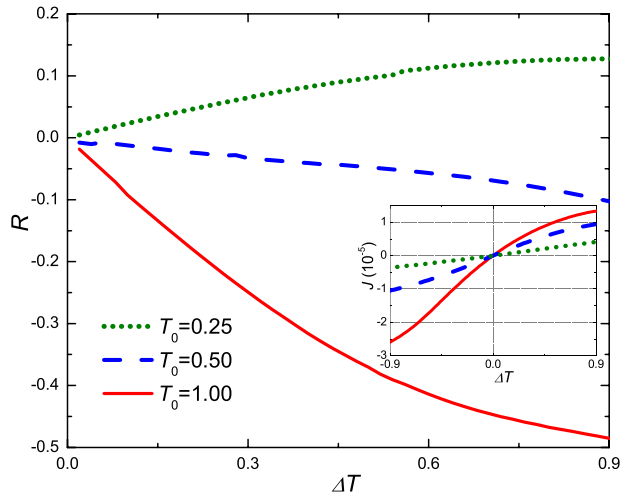

Figure 4. Thermal rectification of the metal–insulator interface versus temperature difference. Inset: thermal current across the interface versus temperature difference. $T_h = T_0(1 + \Delta T)$, $T_c = T_0(1 - \Delta T)$, $V_{ep} = 0.01$.

is several orders of magnitude larger than that through the electron–phonon channel. And even if $\lambda = 4 \times 10^{-4}$ (see the inset of figure 3(b)), the thermal current of the phonon is ten times larger than that of the electron. Therefore for the thermal transport in the non-biased metal–insulator interface, such small thermal current of electron can be ignored, which is consistent with the recent finding in [32]. However, for the interface between a biased metal and a insulator, the thermal transport through the electron–phonon interaction is very important, and dominates the thermal transport even if $\lambda = 1$ as shown in figure 3(a), which can explain the remote Joule heating via electron–phonon interaction in [9].

4. Thermal rectification across the interface via EPI

Thanks to the nonlinearity and asymmetry of the metal–insulator interface, we can expect the thermal rectification, which is defined as $R = (J_+ - J_-)/\max\{J_+, J_-\}$, where J_+ is the forward direction heat flux, defined as $T_L = T_h, T_R = T_c$, and J_- is that of the backward direction when $T_L = T_c, T_R = T_h$. Here, T_h and T_c correspond to the temperatures of the hot and cold baths, respectively. In the rest of the paper, we do not consider the phonon contribution in metal (we set $\lambda = 10^{-4}, T_{Lp} = T_R$ in the calculation to avoid divergence), which will not change the physical properties of the rectification, and only decrease its magnitude. Figure 4 shows the dependence of thermal rectification on temperature difference for different average temperatures. The rectification shows a monotonically increasing behavior of temperature difference due to the bigger difference of heat current in the larger temperature difference as shown in the inset of figure 4, which is consistent with traditional studies on thermal rectification [33–35]. With the temperature T_0 increasing, we find that the rectification can change sign.

The dependence of thermal rectification on temperature and the EPI is shown in figure 5. We find that at a relatively larger EPI ($V_{ep} = 0.01$), with increasing of the temperature, the thermal rectification can change sign from positive to negative. However for a very weak EPI, the rectification always remains negative, as shown in figure 5(b). Within the range of $\lambda = 10^{-4}$–10^{-2}, the rectification is always negative for higher temperatures, while it can change sign from negative to positive at a lower temperature $T = 0.25$. The relation of thermal currents in the forward and backward direction changes with increasing of λ while both their magnitudes monotonically increase, as shown in figure 5(c).

From the locally available density of states (LADOS) of electrons and phonons at the surface of the corresponding leads, we find that at a higher temperature $T_0 = 1.0$, going from the forward transport to the backward one, the main change is that the LADOS of phonons largely increases, as shown in figures 5(d3) and (d4), which causes a larger current in the backward direction than that in the forward direction, and thus the rectification is negative. At a lower temperature, the change of LADOS for electrons and phonons is not obvious, as shown in figures 5(d1) and (d2), and the rectification changes with the strength of EPI.

Turning to the EPI, the electron Green's functions change much more than the phonon ones; with increasing EPI, the Green's functions of electrons $G^>$ and $G^<$ become more asymmetric, especially for the $G^<$ which has a larger value at the energy far away from the Fermi level ($\varepsilon = 0$). At a very weak EPI, the heat current comes from the contribution of electronic energies symmetrically away from the Fermi level. The heat current of the backward transport is larger than that of the forward one, as shown in figures 5(e1) and (e3), due to the increase of the LADOS of phonons in the backward direction, and thus the rectification is negative for all the temperatures at weak EPI as shown in figure 5(b). A stronger EPI induces a larger value of $G^<$ in the energy range -2 to -1, where the center electron has larger density of states. Thus we find that the forward current has a larger value in the range of -2 to -1 as shown in figure 5(e2). At the same time, the heat current can be affected by the temperature: in the low-temperature range, as temperature increases, more electrons with energy far away from the Fermi level contribute to the thermal current, as discussed in figure 2(b). Thus in figure 5(e2), the forward heat current is larger than the backward one; and the rectification is positive at low temperatures with larger EPI. In the higher temperature range, the contribution from energy far away from the Fermi level will decrease with temperature increasing as shown in figure 2(b); furthermore, the main change in the LADOS of electron and phonon is the larger phonon LADOS in the backward transport than that in the forward one; thus the backward heat current is larger than the forward one as shown in figure 5(e4). Therefore, due to the mismatch of electron and phonon LADOS, the rectification is negative for high temperatures or weak EPI. Due to the nonlinearity of EPI and its relation with temperature, we find positive rectification with relatively larger EPI at low temperatures.

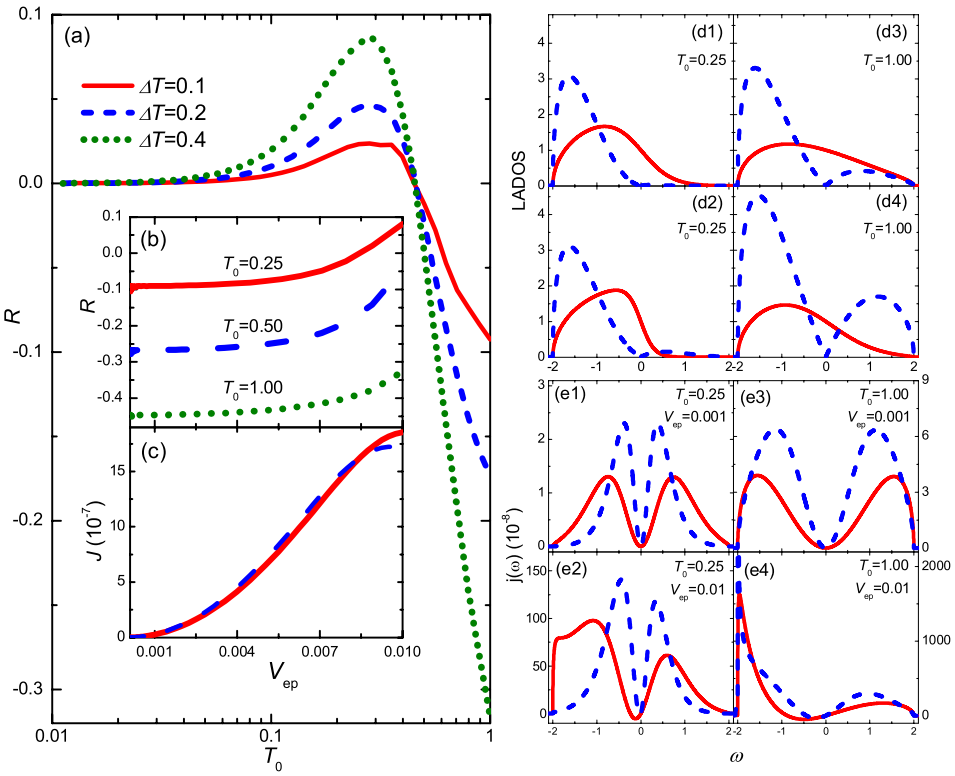

Figure 5. (a) Thermal rectification of the metal–insulator interface versus temperature T_0 for different temperature differences at $V_{ep} = 0.01$. (b) Thermal rectification versus the electron–phonon interaction V_{ep} at different temperatures. (c) The forward thermal current (solid line) and backward thermal one (dashed line) versus V_{ep} at $T_0 = 0.25$. (d1)–(d4) The local available density of states (LADOS) at surface for the left electron part ($\rho_e = |\mathrm{Img}(g^<)|$)(solid line) and the right phonon part ($\rho_p = |\mathrm{Img}(d^<)\omega|$) (dashed line). (d1) ((d2)) and (d3) ((d4)) correspond to the forward (backward) transport at $T_0 = 0.25$ and 1.0, respectively. (e1)–(e4) The forward (solid lines) and backward (dashed lines) thermal current density $J(\varepsilon)$ for different temperatures and different EPI. For all the curves, $T_h = T_0(1 + \Delta T)$, $T_c = T_0(1 - \Delta T)$; from (b) to (e) $\Delta T = 0.4$.

5. Discussions

5.1. Full Green's functions in the calculation

Under the SCBA, we have calculated the self-energies of the EPI; after the iteration convergence we obtain all the Green's functions of $G^{>,<}$ and $D^{>,<}$ in equations (3) and (4), then we can calculate the heat currents. If we do not consider the phonon contribution in the metal part, we should choose the coupling λ to be a very tiny positive value, thus the heat current to the left part will be very small and negligible; as shown in figure 3, if $\lambda = 10^{-4}$ the heat current flowing into the left phonon leads is almost zero. If $\lambda = 0$, the iteration to calculate the self-energies for the EPI will be divergent, but if $\lambda = 0^+ = 10^{-4}$, the iteration is convergent. Thus here the tiny $\lambda = 0^+$ plays a role as a very small onsite potential for the center atom, which is similar as the tiny onsite in computing the phonon Hall effect [36]. We plot the bare Green's functions G_0, D_0 and the full Green's functions G, D in figure 6. Without the EPI, the bare Green's functions of electrons $G_0^<$ and $G_0^>$ are symmetric with respect to the origin as shown in figure 6(a), but the symmetry for $G^<$ and $G^>$ will be broken and change greatly if we turn on the EPI, as can be seen in figure 6(b). However, the Green's functions for phonons do not change much.

5.2. The role of Fermi energy of electrons

We have set the onsite $\varepsilon_0 = 0$ in the main text, thus the Fermi energy of the electron system is $\varepsilon = 0$. However, we can change the onsite ε, as shown in figure 7—the onsite potential can change the magnitude of the thermal conductance and the rectification, and the temperature where the thermal conductance and rectification have maximum value shifts a bit. However, the curves of the thermal conductance and rectification have the same properties as in the case at $\varepsilon_0 = 0$. Therefore, the mechanism found for the nonmonotonicity of conductance and reversal of rectification still holds for the case of nonzero Fermi energy.

5.3. Limitation and application

We have used a simplified one-dimensional model to study thermal conductance and rectification across the metal–insulator interface via electron–phonon interaction. For some quasi-one-dimensional metal–insulator interface systems, the thermal transport can simply be recast as a one-dimensional model, and then our results of the conductance and rectification can be applied. The thermal resistance of an interface system comes from the two materials themselves and the interface between them. Our study in

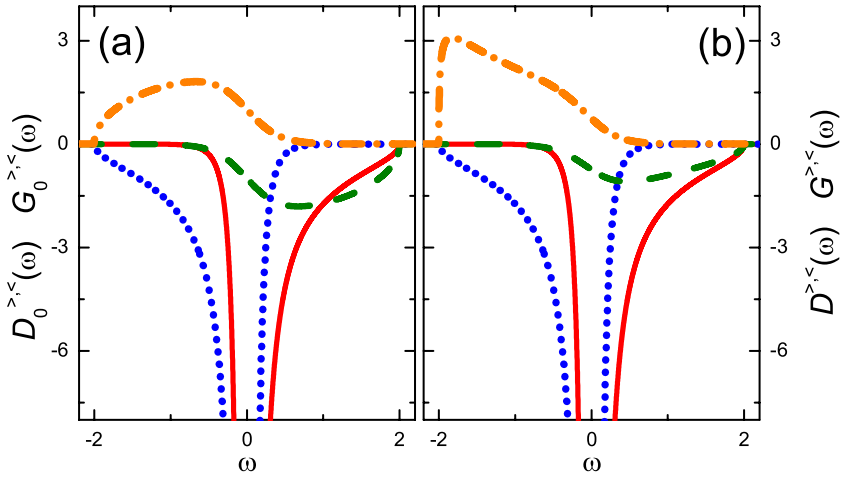

Figure 6. Green's functions for electrons and phonons, $T_{Le} = T_0 + \Delta T$, $T_{Lp} = T_R = T_0 - \Delta T$, $T_0 = 0.2$, $\Delta T = 0.01$. (a) The imaginary part of the bare greater and lesser Green's function for phonons and electrons: $D_0^>$ (solid line), $D_0^<$ (dotted line), $G_0^>$ (dashed line), $G_0^<$ (dash-dotted line). (b) The imaginary part of the full Green's function for phonons and electrons: $D^>$ (solid line), $D^<$ (dotted line), $G^>$ (dashed line), $G^<$ (dash-dotted line) with the EPI ($V_{ep} = 0.01$).

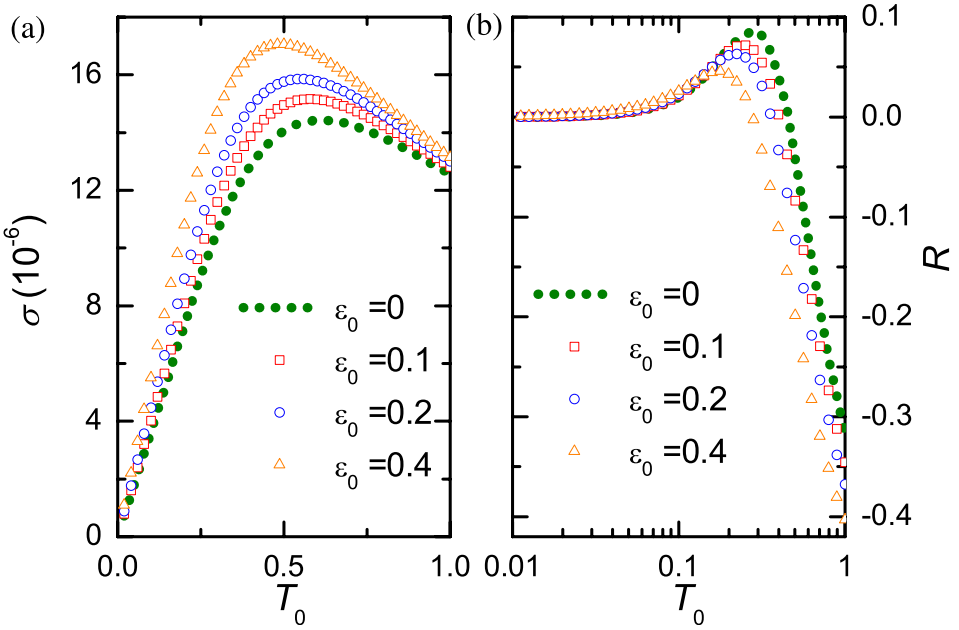

Figure 7. The conductance (left panel) and the rectification (right panel) versus the onsite ε_0. $\lambda = 10^{-4}$. For comparison, the dotted lines in (a) and (b) are copied from the corresponding line in figures 2(a) and 5(a), respectively.

this work focuses on the interface, and provides some understanding on the role of the interface in the thermal transport. Although the thermal transport via electron–phonon interaction can be ignored in the non-biased metal–insulator interface, it dominates the thermal transport in the remote Joule heating in a biased metal–insulator interface.

For real materials, there would be more atoms in one unit cell, thus more phonon branches to contribute to the thermal transport. For comparison with experiments on real materials, the simplified model needs to be generalized to two or three dimensions with input of real parameters. For realistic three-dimensional systems, the density of states of electrons and phonons are quite different from those in one dimension [37], thus the analysis for the mechanism of the thermal rectification would be different and more complicated; but the general properties on the interfacial thermal transport, such as thermal conductance as functions of T, λ and the rectification tuned by temperature or electron–phonon interaction, would still hold and could be verified by future experiments.

The nonequilibrium Green's function approach is a good candidate to solve the interfacial thermal transport. If we study two- or three-dimensional systems with large number atoms in the interface, the self-consistent process is time consuming, and we also need to pay more attention to its convergence. If we only are interested in the thermal conductance accurate to the second order of V_{ep}, the Born approximation is applicable to avoid the convergence problem. However, the

thermal rectification as a function of V_{ep} can only be obtained by the self-consistent Born approximation. Therefore, the calculation of the simple model can provide an understanding of the basic properties of thermal transport at metal–insulator interface and can be generalized to real materials with the parameters obtained from first-principles calculation. Challenges come from the time consuming nature of the self-consistent calculation of the nonlinear self-energies Σ_{ep} and Π_{ep}.

6. Conclusion

In summary, using a nonequilibrium Green's function method we have studied the thermal transport across metal–insulator interface with an EPI. The thermal conductance and rectification across the interface is thoroughly investigated under SCBA by a clean and efficient model where an electron lead couples to a phonon lead through the EPI. We find that the thermal conductance is a nonmonotonic function of average temperature, and it has a maximum value at certain temperature. Considering the phonon part in metal contributing to the thermal transport, the heat flow from the electron part will change while it has a similar dependence on temperature. The thermal rectification effect across the metal–insulator interface can be reversed by varying system average temperature and the EPI. Our results are very helpful to explain and guide experiments on the thermal transport and dissipation in electronic devices and the interface system, and could be verified in the biased and non-biased graphene sheet supported on insulating substrate. The reversal rectification is significant for the study of one-way heat transport and tuning the direction of thermal transport; thus it could have wide application in energy science.

Acknowledgments

LZ and BL are supported by the grant R-144-000-300-112 from Ministry of Education of Republic of Singapore. J-SW acknowledges support from a URC research grant R-144-000-257-112 of NUS. J-TL acknowledges funding support from NSFC with project no. 61371015 and 11304107. BL is also supported by NSF China through project 11334007.

References

[1] Vankatasubramanian R, Silvola E, Colpitts T and O'Quinn B 2001 *Nature* **413** 597
[2] Cahill D G, Ford W K, Goodson K E, Mahan G D, Majumdar A, Maris H J, Merlin R and Phillpot S R 2003 *J. Appl. Phys.* **93** 793
[3] Costescu R M, Cahill D G, Fabreguette F H, Sechrist Z A and George S M 2004 *Science* **303** 989
[4] Majumdar A and Reddy P 2004 *Appl. Phys. Lett.* **84** 4768
[5] Castro Neto A H, Guinea F, Peres N M R, Novoselov K S and Geim A K 2011 *Rev. Mod. Phys.* **81** 109
[6] Little W 1959 *Can. J. Phys.* **37** 334
[7] Chen J H, Jang C, Xiao S, Ishigami M and Fuhrer M S 2008 *Nature Nanotechnol.* **3** 206
[8] Perebeinos V, Rotkin S V, Petrov A G and Avouris P 2009 *Nano Lett.* **9** 312
[9] Baloch K H, Voskanian N, Bronsgeest M and Cumings J 2012 *Nature Nanotechnol.* **7** 316
[10] Swartz E and Pohl R 1989 *Rev. Mod. Phys.* **61** 605
[11] Stevens R, Smith A and Norris P 2005 *J. Heat Transfer* **127** 315
[12] Lumpkin M E and Saslow W M 1997 *Phys. Rev.* B **17** 4295
[13] Wang J and Wang J-S 2006 *Phys. Rev.* B **74** 054303
[14] Zhang L, Wang J-S and Li B 2008 *Phys. Rev.* B **78** 144416
[15] Li B, Lan J and Wang L 2005 *Phys. Rev. Lett.* **95** 104302
[16] Termentzidis K, Chantrenne P and Keblinski P 2009 *Phys. Rev.* B **79** 214307
[17] Landry E S and McGaughey A J H 2009 *Phys. Rev.* B **80** 165304
[18] Haug H and Jauho A P 1996 *Quantum Kinetics in Transport and Optics of Semiconductors* (Berlin: Springer)
[19] Zhang W, Fisher T S and Mingo N 2007 *Numer. Heat Transfer* B **51** 333
[20] Wang J-S, Wang J and Lü J T 2008 *Eur. Phys. J.* B **62** 381
[21] Zhang L, Keblinski P, Wang J-S and Li B 2011 *Phys. Rev.* B **83** 064303
[22] Zhang L, Wang J-S and Li B 2009 *New J. Phys.* **11** 113038
[23] Lü J T and Wang J-S 2007 *Phys. Rev.* B **76** 165418
[24] Galperin M, Ratner M A and Nitzan A 2007 *J. Phys.: Condens. Matter* **19** 103201
Galperin M, Nitzan A and Ratner M A 2007 *Phys. Rev.* B **75** 155312
[25] Musho D and Walker D G 2011 *ASME Conf. Proc. 2011* p 413
[26] Pop E, Mann D A, Goodson K E and Dai H 2007 *J. Appl. Phys.* **101** 093710
[27] Ordonez-Miranda J, Alvarado-Gil J J and Yang R 2011 *J. Appl. Phys.* **109** 094310
[28] Meir Y and Wingreen N S 1992 *Phys. Rev. Lett.* **68** 2512
[29] Jauho A-P, Wingreen N S and Meir Y 1994 *Phys. Rev.* B **50** 5528
[30] Wang J-S, Zeng N, Wang J and Gan C K 2007 *Phys. Rev.* E **75** 061128
[31] Chen Z, Jang W, Bao W, Lau C N and Dames C 2009 *Appl. Phys. Lett.* **95** 161910
[32] Singh P, Seong M and Sinha S 2013 *Appl. Phys. Lett.* **102** 181906
[33] Li B, Wang L and Casati G 2004 *Phys. Rev. Lett.* **93** 184301
[34] Li N, Ren J, Wang L, Zhang G, Hänggi P and Li B 2012 *Rev. Mod. Phys.* **84** 1045
[35] Zhang L, Yan Y, Wu C-Q, Wang J-S and Li B 2009 *Phys. Rev.* B **80** 172301
[36] Wang J-S and Zhang L 2009 *Phys. Rev.* B **80** 012301
[37] Asai Y 2008 *Phys. Rev.* B **78** 045434